CrystEngComm

Accepted Manuscript

ROYAL SOCIETY OF CHEMISTRY

www.rsc.org/crystengcomm

Cite this: DOI: 10.1039/c0xx00000x

www.rsc.org/xxxxxx

ARTICLE TYPE

Synthesis of curtain like crumpled boehmite and γ-alumina nanosheets

Je-Ruei Wen,[a] Ming-Han Liu[b] and Chung-Yuan Mou*[a,b]

Received (in XXX, XXX) Xth XXXXXXXXX 20XX, Accepted Xth XXXXXXXXX 20XX
DOI: 10.1039/b000000x

Boehmite (γ-AlOOH) nanosheets with curtain-like crumpled morphology have been synthesized via template-free hydrothermal process in two-stages. The formation of the crumpled 2D nanostructure was studied at 80-95 ℃ of stage-1 and 150 ℃ of stage-2 hydrothermal processes, and a growth mechanism is proposed. The introducing of corrugations and wrinkles prevents the nanosheets from severe interface stacking. Based on the XRD, TEM, and N_2 sorption analysis results, the thickness of the nanosheets is ca.2.5-5 nm, which composed of 2-4 lattice unit layers only. The crumpled boehmite nanosheets exhibit high BET surface area of ca. 330 m^2/g, and can be simply transformed into γ-Al_2O_3 with preservation of the morphology and ~90% of surface area after calcination.

1. Introduction

Recently, extensive researches are directed to develop inorganic nanosheets with unique physical and chemical properties.[1,2] The range of applications of nano-assemblies could be broadened significantly for its large surface area, specific surface and pore structures. Compared to the physicochemical properties of graphene, those of inorganic nanosheets have been much less explored. Difficulties in making inorganic nanosheets of large dimension are the roadblocks in realizing their applications. Up to the present, nanosheets of large domain size are mostly made by exfoliation of layered materials, a top-down approach. However, exfoliation method does not work for many strong binding layered materials. A bottom-up synthetic approach for inorganic nanosheets would be most desirable. In this paper, we would like to report on a synthetic approach for solution fabrication of boehmite of crumpled nanosheet form that has large surface area and large domain size.

Boehmite, aluminum oxyhydroxide (γ-AlOOH), is a layer-structured material with the layers linked by hydrogen bonds and stacked along [010].[3] It has been widely used as adsorbents,[4-6] catalyst supports,[7,8] ceramics,[9] and superhydrophobic films.[10,11] It is also a precursor of gamma-alumina (γ-Al_2O_3), which is an important material in heterogeneous catalysis. Boehmite undergoes an isomorphous phase transformation to γ-Al_2O_3 by simply dehydration above ca. 400 □, and the resulting product can retain the morphology of the parent boehmite.[12] Accordingly, controlling of boehmite morphology is of great interest that it governs the terminated facets of final alumina product and the corresponding acid-basic properties,[13] which play critical roles for adsorbent, catalyst, and catalyst support applications. Over the past decade, boehmite with numerous kinds of morphology have been reported, such as nanorods,[14-16] nanowires,[17] nanofibers,[18] nanotubes,[19-21] nanoplates,[22-25] nanobelts,[5] bunches of aligned nanowires,[12] cantaloupe-like structures,[26] flower-like structures,[7,27-31] and hollow spheres.[32-35] After calcination treatment, however, serious aggregation or sintering are typically encountered for nanomaterials. Therefore preservation of both fine morphology and high surface area has long been a matter of concern. On the other hand, hydrothermal synthesis of boehmite, one of the most used approaches, has the advantages of controlling the size, shape, and crystallinity. Factors in managing the boehmite crystal growth through hydrothermal method are aluminum source, counteranion, directing agent, solvent, pH environment, and reaction temperature.

Up to the present, there are few studies about boehmite with nanosheet structure of large dimension and thin thickness. The few reported cases are mostly in small flake form.[36,37] In this work, we report a two-stage hydrothermal route to synthesize boehmite having a curtain-like crumpled nanosheet morphology of large dimension without additional capping agent or co-solvent. The great feature of this crumpled nanosheet form is its three-dimensional extension in space which avoids serious stacking. The undulating ruffles and wrinkles over the nanosheets greatly prevent the nanosheets from severe interface stacking. This allows us to obtain nanosheets form of γ-Al_2O_3 of high surface area after calcination of the boehmite nanosheet samples. The effects of the hydrothermal processes are investigated, and the growth mechanism is studied.

2. Experimental

2.1 Synthesis

All of the reagents were analytical grade purchased from Acrös and used without further purification. In a typical preparation, 0.8247 g of $Al_2(SO_4)_3 \cdot 18H_2O$ was dissolved into 100 mL distilled water, adjusting the pH to 2.50 by addition of diluted sulfuric acid. The solution was transferred into a round flask, heating to 70 ℃ in oil bath with vigorous stirring, then desired amount of 2M hexamethylenetetramine (HMTA) aqueous solution was added drop by drop. The heating profile of the

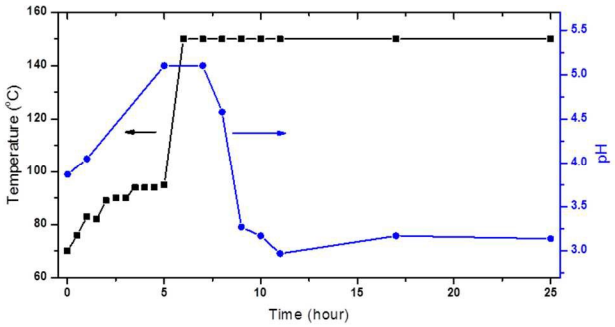

Fig. 1 The reaction time versus the reaction heating profile and the corresponding pH value.

whole hydrothermal process is given in Figure 1. In stage-1 hydrothermal procedure, the mixed solution was heated from 70 to 95 ℃ in 5 hours gradually. In stage-2 process, the formed precipitant and suspension were transferred into Teflon-lined stainless steel autoclaves with 80% fill of total volume and subsequently heating to 150 ℃ and keeping for 20 hours. At the same time, pH value of the solution was continuously monitored as shown in Figure 1. After the hydrothermal treatment, the autoclaves were cooled to room temperature. The resulting precipitate was collected by filtration and washed with distilled water and absolute ethanol, and finally dried in air at 60 ℃ overnight. For comparison, $AlCl_3 \cdot 6H_2O$ and $Al(NO_3)_3 \cdot 19H_2O$ were used as substitutes of aluminum resource with diluted HCl and HNO_3 for adjusting the initial pH values respectively, while all the other reaction conditions remained the same.

To obtain crumpled alumina nanosheets, the synthesized boehmite samples were calcined in atmospheric circumstance at 500-900 ℃, with a heating rate of about 1.5 ℃/min for 4 h.

2.2 Characterization

Powder X-ray diffraction (XRD) was performed on a PANalytical's X'PertPRO X-ray diffractometer using filtered Cu Kα radiation (λ = 0.154 nm). The crystal size of boehmite was calculated using the Scherrer equation: $\tau = (0.9\lambda)/(\beta \cos \theta)$, where τ, λ, β, and θ are the crystallite size, X-ray (Cu Kα) wavelength, full width at half-maximum intensity (FWHM) of individual peak in radians, and Bragg's diffraction angle respectively. Fourier transform infared (FTIR) spectroscopy was conducted by a BRUKER VERTEX 70. Samples were pelletized with KBr by a volume ratio of about 1:9. Transmission electron microscopy (TEM) images were taken on a JEOL JSM-1200 EX II operating at 100 kV. Samples were first dispersed in absolute ethanol, and were dropped on carbon-coated copper grids. Scanning electron microscopy (SEM) images were taken on a JEOL JSM-7600F Field Emission Scanning Electron Microscope. High-resolution transmission electron microscopy (HRTEM) images were taken on a Tecnai 20 G2 S-Twin operating at 200 kV. Nitrogen adsorption-desorption isotherms were measured at 77 K with Micromeritics ASAP2010. The samples were degassed at 110 ℃ for 1 day under 5×10^{-3} torr before analysis. The specific surface areas were calculated by Brunauer-Emmett-Teller (BET) method. Zeta potential analysis was performed on a Molvern Zetasizer Nano ZS (Malvern, UK). The

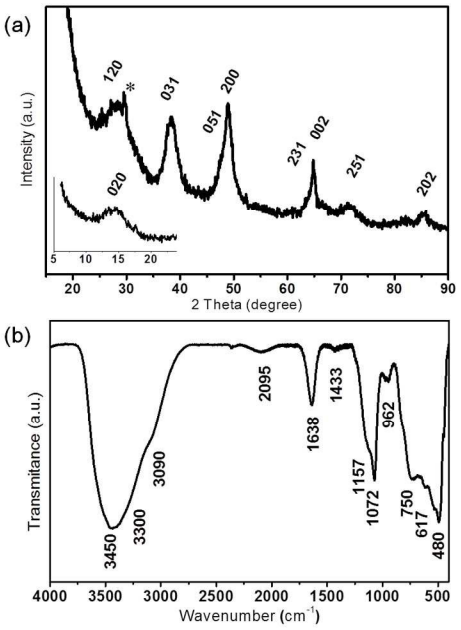

Fig. 2 (a) XRD pattern and (b) FTIR spectrum of the as-prepared sample.

compositions of suspensions after the reaction were examined by a Clarus 600/560 D gas chromatograph-mass spectrometry (GC-MS). The GC column phase reference is 5% diphenyl 95% dimethyl polysiloxane. The GS-MS conditions were as follows: Injector Port Temperature: 250 ℃; Column Temperature: Initial Temperature: 35 ℃ (2 min); Gradient Rate: 15 ℃/min (8 min); Final Temperature: 155 ℃ (hold for 1 min); Flow Rate: 1 mL/min. The concentrations of aluminum in the leak test were analyzed by inductively coupled plasma mass spectrometry (ICP-MS) using an Agilent 7700e ICP-MS. In a typical leak test, 30 mg of sample was added into 30 mL distilled water, followed with adjusting the pH ranging from 2.50 to 5.00 by diluted sulfuric acid or nitric acid. The solution was kept at 30 ℃ with magnetic stirring for 24 hours. The suspension was subsequently collected by centrifuging at 12000 rpm for 15 min and then filtering through a 0.45 μm PVDF membrane, and was properly diluted with 2 wt% nitric acid before analyzing.

3. Results and discussion

3.1 Structural properties

Powder XRD was used to examine the phase of the product. Figure 2a shows the XRD pattern of the as-prepared sample after the two-stage hydrothermal process. Most diffraction peaks can be indexed to orthorhombic γ-AlOOH (JCPDS No. 21-1307) except a tiny peak at 29.7°, which belongs to ammonioalunite ($(NH_4)Al_3(SO_4)_2(OH)_6$) (JCPDS No. 42-1334). The formation of γ-AlOOH is also evidenced by the FTIR spectrum as shown in Figure 2b. The three bands at 480 cm^{-1}, 617 cm^{-1}, and 750 cm^{-1} are assigned to δ Al-O, ν Al-O, and torsional mode of AlO_6 octahedra of boehmite.[20] The band at 1072 cm^{-1} and the shoulder at ~1157 cm^{-1} can be assigned to δ_s Al-O-H and δ_{as} Al-O-H respectively. The broad band around 3450 cm^{-1} is assigned to stretching mode of OH groups in the oxyhydroxide structure and physisorbed water, and the two shoulders appeared at 3300 cm^{-1} and 3090 cm^{-1} represent ν_{as} (Al)O-H and ν_s (Al)O-H stretching

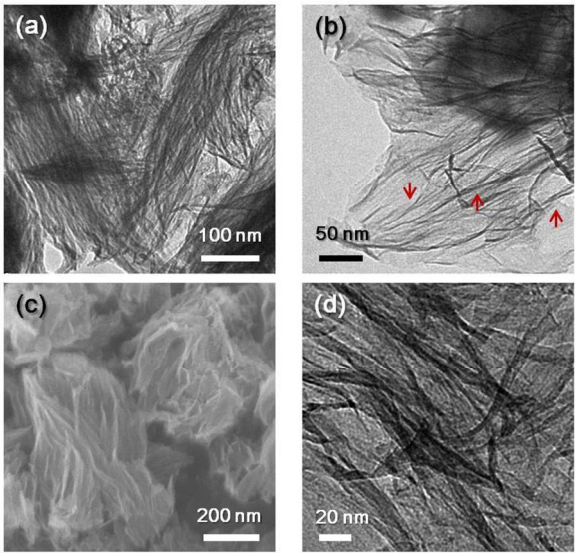

Fig. 3 (a,b) TEM, (c) SEM and (d) HRTEM images of crumpled boehmite nanosheets.

Table 1 Crystallite size derived from TEM image and XRD patterns.

data source	TEM wrinkle	XRD (020)	XRD (200)	XRD (002)
crystal size (nm)	2.5-5	2.23	5.06	11.3

modes of γ-AlOOH. The weak band at ~2095 cm^{-1} is the combination band, and the intense band at 1638 cm^{-1} is attributed to the bending mode of adsorbed water.[26] In addition, a small band at 1433 cm^{-1} may come from NH_4^+ bending mode of trace amount of ammonioalunite.[38] While a tiny band at 962 cm^{-1} may come either from ν_1 SO_4 or Al-OH_2 bending mode,[39] it disappears after calcination in air environment at 280℃ (Figure S2e).

3.2 Morphology

The morphology of the sample was studied by TEM, SEM, and HRTEM. TEM images in Figure 3a,b display that the boehmite product is an agglomerates of extremely thin nanosheets with lateral dimension of about hundreds of nanometers. The nanosheets are so thin that they are intensely crumpled with wrinkles approximately parallel to each other in a curtain-like fold. It is worth noting that some of the wrinkles merge together along a certain direction (as indicated by arrows in Figure 3b), making the nanosheet highly corrugated in one side but less in the other side, just like the drapes of a curtain. The SEM image in Figure 3c corroborates the aggregated crumpled nanosheet appearance, and the oriented folds are clearly observed. Such nanoarchitecture is responsible for the broadened XRD peaks (Figure 2a), the introducing of folds and wrinkles caused distortion of lattice structure around bended regions, leading to poor crystallinity.

When taking a closer look at an individual curtain-like crumpled nanosheet by high-resolution TEM, as shown in Figure 3d, folds, wrinkles, and their joints can be clearly seen. The widths of folds are mostly in range of 5-10 nm, e.g. the thickness of a single nanosheet should be at about 2.5-5 nm. It has been reported that boehmite crystal usually exposes the low index surfaces of (100), (010), (001) and (101), with the (010) surface possessing the lowest surface energy.[40,41] The crystallite sizes of our crumpled boehmite nanosheets as calculated from the XRD pattern in Figure 2a are summarized in Table 1. It shows that the crystal dimension along [020] direction is the smallest one, of only 2.23 nm, which is close to the thickness of crumpled nanosheets estimated from the folds observed in HRTEM image. This suggests the nanosheets were grown anisotropically along xz plane, exposing the OH-abundant (010) surface. Moreover, since the boehmite lattice constant of b axis is 12.21 Å,[42] the nanosheets are of only 2 to 4 crystal lattice in thickness.

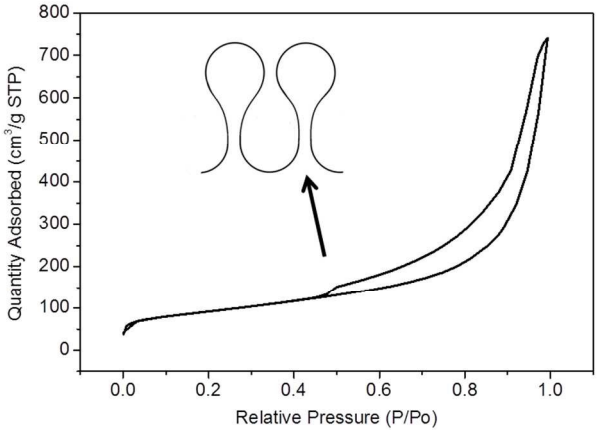

Fig. 4 BET of crumpled boehmite nanosheets. The inset illustrates the origin of pore blocking phenomenon around P/P_0 0.45-0.5 causing the hysteresis behaviour.

3.3 Surface property

The crumpled boehmite nanosheets were further studied by N_2 sorption analysis. As can be seen from Figure 4, the sample displays a type II isotherm with a H3 type hysteresis loop. Since the H3 type hysteresis is usually observed in plate-like particles giving rise to slit-like pores, the loop does agree with the nanosheet form of our sample. The sorption hysteresis around P/P_0 0.45-0.5 indicates the existence of large confined volume between the crumpled nanosheets, which may be attributed to the corrugations giving U-shaped cavities and bottlenecks (see the inset of Figure 4).

The BET specific surface area calculated from the isotherm is 328.8 m^2/g, 2 to 3 times higher than those reported for 3D structures assembled from nanopetals[28] and nanoflakes[34], and an order higher than those of 2D nanobelts and nanoplates.[5] Such a high surface area of our boehmite nanosheets may be ascribed to the thin thickness and the crumpled morphology that prevents tight stacking between nanosheets. Assuming exposed (010) plane with various thickness, we estimated the surface area of boehmite (see ESI for details). The calculation gives that boehmite sheet with only one-lattice thick has a surface area of 529 m^2/g, and the surface areas are about 353 m^2/g and 265 m^2/g for sheets with thickness of 1.5- and 2-lattices length respectively. The crumpled boehmite nanosheets with the high experimental surface area correspond to nanosheets of 1.5- to 2-lattice thick, which is consistent with the estimates from XRD and HRTEM.

3.4 Growth evolution

To understand the formation of the unique morphology, samples

at different synthesis stages were collected and characterized by

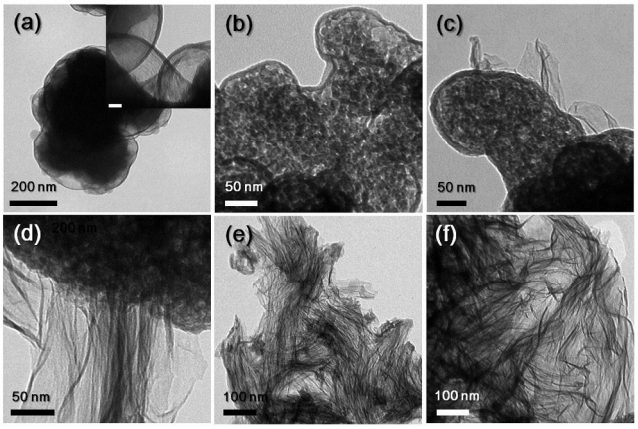

Fig. 5 TEM images of sample derived at different times : (a) 1, (b) 5, (c) 5+2, (d) 5+3, (e) 5+4, and (f) 5+6 h. The 5+x h means that the sample was collected after n hours of second hydrothermal treatment (ex: 5+2 h denotes the sample was obtained at reaction time of 7 h in Figure 1). The scale bar of the inset in (a) is 20 nm.

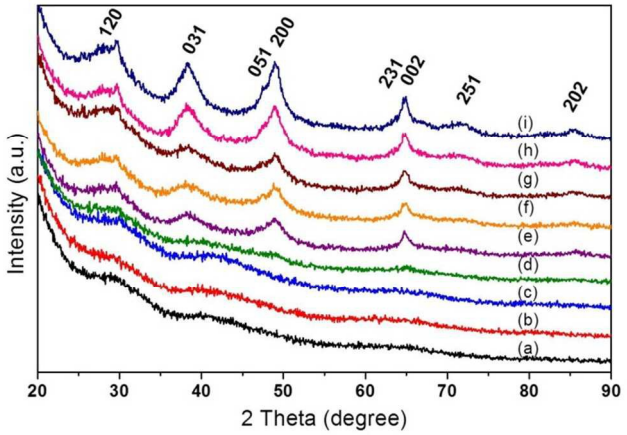

Fig. 6 XRD patterns of samples derived at different times: (a) 1, (b) 5, (c) 5+2, (d) 5+3, (e) 5+4, (f) 5+5, (g) 5+6, (h) 5+12 and (i) 5+20 h.

TEM, XRD, FTIR, and zeta-potential analysis. As can be seen in Figure 5a and Figure S1a, an abundant aggregated hollow particles with interior cores having diameter of about 100-300 nm were obtained after 1 h hydrothermal treatment in stage-1. In Figure 5a, it is clear that the particles were composed of ~10 nm thick shells and featureless cores. At increasing reaction time of 5 h in stage-1 (Figure 5b), the cores were transformed into discrete nanoclusters while the shells remained. The materials up to this stage are of amorphous nature (Figure 6a,b), and are assigned as polymeric Al-SO_4 complexes and amorphous aluminum hydroxide ($Al(OH)_3$),[34,39] which can be evidenced by FTIR and zeta-potential analysis (Figure S2 and S3).

When the reaction proceeded to 5+2 h in stage-2 hydrothermal process at 150 ℃, XRD pattern of the sample still gave no discriminable XRD reflections (Figure 6c). However, as demonstrated in the TEM micrographs (Figure 5c and Figure S1b), a few small and thin nanosheets of about 50 nm in length began to grow at the shell surface, and the isoelectric point (IEP) value rose abruptly from ~7.4 at 5 h to over 9 which is close to that of typical boehmite materials (Figure S3).[23] With the reaction prolonging to 5+3 h, the shells disappeared, while the nanosheets extended to hundreds of nanometers and reached to the inner core (Figure 5d and Figure S1c). More importantly, the

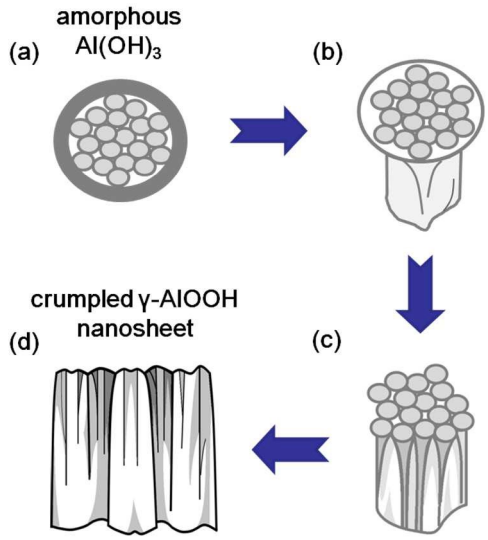

Scheme 1 Schematic illustration of morphology evolution for crumpled boehmite.

nanosheets became intensely crumpled with the corrugations approximately vertical to the core. The corrugations are more crowded at the root, e.g. the boundary between core and nanosheet, gradually merging together and becoming more expanded edge. Meanwhile, the XRD pattern showed faint but sharper peaks (Figure 6d), and the FTIR spectra illustrated that the bands of octahedral AlO_6 and tetrahedra AlO_4 converted into one broad band (Figure S2), indicating that the morphology conversion was accompanied with phase transformation. The XRD patterns in Figure 6e could be indexed to orthorhombic γ-AlOOH, as the reaction ran to 5+4 h. The obtained product displayed the formation of many crumpled nanosheets, while the clustered cores were barely observable (Figure 5e and Figure S1d). When the reaction proceeded to 5+6 h, no more clustered core could be found, only the crumpled nanosheets were observed (Figure 5f). Thereafter, the products exhibited nearly identical morphology even after prolonged reaction (figures not shown). Nevertheless, Figures 6f-i demonstrate sharper XRD patterns, suggesting that the crystallinity improved with longer hydrothermal treatment. Furthermore, the zeta-potential analysis gave an IEP value of 10.1 of the final product (Figure S3), a little higher than that of bulk boehmites. The high IEP value is considered as a result of the unique crumpled morphology. Because of the abundance of high curvature regions, the boehmite material may expose significant amount of low-coordinated Al atoms, such as Al_{IV} and Al_{III}, making the charges of crumpled nanosheets surface more positive.[40]

3.5 Proposed growth mechanism

From the studies above, we would like then to discuss the underline mechanism in the formation of boehmite nanosheets. At the same time, we need to understand the chemical reactions involved in the time-evolution behavior of pH during synthesis (Figure 1). The proposed mechanism is summarized in Scheme 1 as the synthesis goes along in time. At the beginning of stage-1, hydrolysis of HMTA generated formaldehyde and ammonia[43]

(eq. (1)) which caused the pH condition to rise. When the pH is high enough, precipitation of the irregular aluminum hydroxide core-shell particle intermediate occurred (eq. (2)).

$$C_6H_{12}N_4 + 6\ H_2O \rightarrow 4\ NH_3 + 6\ CH_2O \quad (1)$$

$$Al^{3+} + 3\ H_3^+O + 6\ NH_3 \rightarrow Al(OH)_3 + 6\ NH_4^+ \quad (2)$$

$$Al(OH)_3 \rightarrow \gamma\text{-}AlOOH + H_2O \quad (3)$$

$$2\ CH_2O + H_2O \rightarrow HCOOH + CH_3OH \quad (4)$$

As the hydrothermal treatment continued, further hydrolysis of HMTA makes the solution more basic. The aluminum species probably underwent a polycondensation reaction, forming the clustered nanostructures in the core. When the temperature was raised to 150 ℃ at the second stage, the high temperature and pH circumstance drove the phase transformation of aluminum hydroxide to boehmite[20] (eq. (3)). The reaction began from the exterior of the particles that the aluminum hydroxide dissolved then recrystallized at the shell surface. Because of the known selective adsorption of sulfate ions[15,23,34] on the (010) surface, the growth of boehmite crystals was strongly hindered in the [010] direction and thus facilitated the formation of nanosheet morphology. After the shells were consumed, the boehmite nanosheets reached to the cores. The interaction between the nanosheets and the clustered cores created strain on the nanosheets, which caused the deformation of flat sheet into the crumpled morphology, resembling the formation of drapes in a hanging curtain. As the phase transformation continued, the nanosheets anisotropically grew larger and larger, and finally the curtain-like crumpled boehmite nanosheets were obtained.

For comparison, we have also used $AlCl_3$ and $Al(NO_3)_3$ as aluminum sources. As shown in Figure S4, assemblies of nanoplates with thickness about 20 nm were produced. These nanoplates are evidently much thicker and smaller in lateral dimensions in contrast to the crumpled nanosheets using aluminum sulfate, verifying the morphology-directing role of sulfate ions. In addition, during the stage-2 hydrothermal treatment, it was found that the pH value of the solution dropped abruptly from 5.1 at 5+2 h to around 3 after 5+4 h. This phenomenon cannot be explained by the simple hydrolysis of HMTA in eq. (1). We propose that the drop of pH value was caused by the disproportional reaction of formaldehyde to formic acid and methanol at high temperature, as given in eq. (4). To show this, suspension of the final product was characterized by GC-MS to examine volatile organic products. Also, a controlled experiment was conducted that hydrothermal treatment of formaldehyde along with ammonium sulfate was carried out at 150 ℃. As shown in Figure S5, substantial amount of methanol was detected in both the suspension and the controlled sample. We could not directly detect formic acid in GC since its salt is not volatile. However, the formation of methanol is the evidence that the disproportion reaction (eq. (4)) did occur, implying the production of formic acid during the process.

The drop of pH at high temperature, due to formation of formic acid, is a critical factor in forming the distinctive architecture in our system. Under the low pH reaction condition at stage-2, boehmite was highly positively charged (Figure S3), which made the nanosheets repulsive to each other and facilitated the strong adsorption of sulfate ions at the same time. Therefore the layer-stacking aggregation was avoided and eventually the extremely

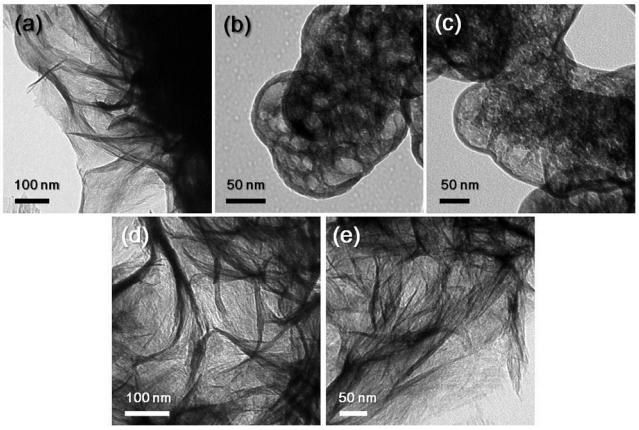

Fig. 7 TEM images of sample prepared by different stage-1 conditions: (a) without stage-1, (b) 85 ℃ for 5 h, (c) 95 ℃ for 5h, (d,e) the final products of (b) and (c) after subsequent stage-2 hydrothermal treatment at 150 ℃ respectively.

thin nanosheets were formed. Since the pKa value of formic acid is 3.77, the solution is buffered around pH~3 value in the 2nd stage of our synthesis. The buffer action stopped pH from decreasing below 3. Otherwise, one would obtain different products of ammonioalunite or basic aluminium sulfate ($(H_3O)Al_3(SO_4)_2(OH)_6$).[44,45] According to Xia et al,[45] the formation process of basic aluminium sulfate undergoes a dissolution-recrystallization mechanism that boehmite dissolves at high H^+ concentration condition then recrystallizes as basic aluminium sulfate. We believe the formation of small quantity of ammonioalunite, as evidenced in Figure 1 and 2, follows a similar pathway under the pH environment as low as 3.12 in our case. Even so, the solubility of boehmite is quite low around pH 3-4 at elevated temperature,[46] the dissolution of whole boehmite material is not favored in the reaction that contributed to the maintenance of the unique morphology without undergoing Ostwald ripening nor further phase transformation into ammonioalunite. Yet, it is still astonishing that such nanosheet structure as thin as 2.5 nm could be stable under such low pH circumstance.[47] In order to further validate the stability of the crumpled boehmite nanosheets, dissolution of aluminum from the obtained sample was tested against sulfuric acid and nitric acid at the pH rage from 2.5 to 5.0. It was found that the leaching of aluminum is extremely low in sulfuric acid solution, less than 0.02 % were dissolved at pH 3 (Figure S6). The crumpled boehmite nanosheets show an order of magnitude lower dissolution in sulfuric acid than in nitric acid. This verifies the stabilizing effect of sulfate ions as well.

3.6 Effect of stage-1 hydrothermal process

To elucidate the distinction of the two-stage hydrothermal process, experiment without stage-1 hydrothermal process, e.g. direct one-step hydrothermal procedure at 150 ℃ was performed. TEM image in Figure 7a shows the boehmite material has nanosheet morphology as well but evidently less crumpled. The difference between samples with and without stage-1 hydrothermal process is particularly discernible in N_2 adsorption-desorption isotherms. In Figure S7b, boehmite without stage-1

reveals similar type II isotherm, though, it has significantly smaller hysteresis around P/P_0 0.45 to 0.8. Also, the one-stage derived boehmite exhibits smaller specific surface area of

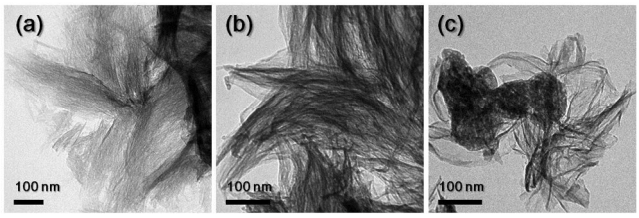

Fig. 8 TEM images of sample derived with stage-2 hydrothermal temperature at (a) 180 ℃,(b) 120 ℃ and (c) 105 ℃.

258.3 m^2/g. These distinctions can be attributed to less crumpling in nanosheets of samples without stage-1 treatment which yields less cavity between the corrugations, and stacking between nanosheets could occur and bring on reduction of the surface area.

More experiments of adjusting the heating procedure in stage-1 hydrothermal process were studied. The stage-1 processes of controlled experiments were conducted at 80 ℃ and 95 ℃ for 5 hours. At 80 ℃ for 5 h (Figure 7b), no well-defined cluster was formed in the core. At 95 ℃ for 5 h (Figure 7c), the clusters are clearly seen but have an uneven distribution, especially gathering in the middle. After the stage-2 treatment at 150 ℃, both the final products show less crumpled structures (Figure 7d,e). The N_2 sorption isotherms of the two samples in Figure S7c,d display tiny hysteresis loops around P/P_0 of 0.5, and their BET surface areas are 267.5 m^2/g and 277.3 m^2/g respectively, verifying the less crumpled nature. The findings suggest the critical role of stage-1 hydrothermal procedure controlling the intermediate core-shell particles on which boehmite nanosheets subsequently grow. As mentioned above, the amorphous aluminum hydroxide particles act as sacrificial template that determines the lattice strain, hence the stage-1 hydrothermal process influences the generation of folds and wrinkles in the next stage. Stage-1 gives the very small baseline of curtain from which the nanosheets became highly crumpled.

3.7 Effect of stage-2 hydrothermal process

It is known that the phase transformation from aluminum hydroxide to aluminum oxyhydroxide during hydrothermal treatment is temperature-dependent. Accordingly the effect of reaction temperature over the stage-2 hydrothermal process was investigated from 180 ℃ to 105 ℃, and the XRD patterns of the corresponding products are shown in Figure S8. Samples synthesized at 180 ℃ and 120 ℃ exhibited fine XRD pattern of γ-AlOOH (with a minute peak of ammonioalunite at 29.7°) and gave increased intensity with increasing hydrothermal temperature. However, sample prepared at 105 ℃ displays hardly distinguished diffraction pattern. The TEM image of sample obtained at 180 ℃ demonstrates a mixture of crumpled nanosheets and nanowires (Figure 8a). The nanowires are 10-20 nm in diameter and hundreds of nanometers in length. Sample synthesized at 120 ℃ displays curtain-like crumpled nanosheet morphology (Figure 8b), resemble that obtained at 150 ℃ (Figure 3). Besides, irregular particles with attached moderately crumpled nanosheets are produced at 105 ℃ (Figure 8c). It is noticed that both the TEM and XRD results of this 105 ℃-derived sample are similar to what achieved at 150 ℃ for 3 h (Figure 5d and 6d), suggesting the particles are supposedly amorphous $Al(OH)_3$ and the nanosheets are poorly crystallized γ-AlOOH.

N_2 adsorption-desorption isotherms of the samples exhibit type II isotherms and H3 loops (Figure S9), the hysteresis loops are quite different however. The 120 ℃-synthesized sample gives enormous hysteresis around P/P_0 of 0.5, while the loop of the sample formed at 180 ℃ is evidently smaller, and becomes extremely tiny for sample prepared at 105 ℃. The BET surface areas are 285.5, 266.2, and 32.57 m^2/g for samples derived at 180 ℃, 120 ℃, and 105 ℃ respectively in agreement with XRD and TEM observations. It can be concluded that in the second hydrothermal procedure, the high temperature drives the phase transition reaction, but only within an appropriate temperature range can the crumpled nanosheets be fabricated. At higher stage-2 temperature, the fast reaction rate would facilitate the formation of small crystal and favor product with more thermodynamically stable shape, hence strips of nanowires are collected along with nanosheets. At lower temperature, on the contrary, the reaction condition does not provide sufficient driving force, giving rise to the incomplete phase transformation reaction of aluminium hydroxide.

3.8 Comparison with previous synthesis of boehmite

Before this work, several studies have reported boehmite with sheet-like morphology: Cai et al.[36] applied an azeotropic distillation-assisted method to produce boehmite nanofibers of crumpled sheet-like morphology. Frost and co-workers[21] prepared a mixture of nanotubes and featureless boehmite by hydrothermal method with the aid of poly(ethylene oxide) (PEO) as soft template. Agglomerated γ-AlOOH lamellas have been reported by Logar et al.,[8] utilizing the hydrolysis of aluminum nitride (AlN) powder. Xu el al.[37] synthesized mesoporous aluminum oxyhydroxide nanoflakes via a water-in-oil microemulsion-assisted hydrothermal process by addition of cyclohexane and polyethylene glycol (PEG). Chen el al.[17] fabricated straw-bundle-like boehmite architectures using $Al(NO_3)_3 \cdot 9H_2O$ as aluminum source and urea as base. Different from the boehmite materials prepared by previous groups, the boehmite in our work was originated by crumpling of nanosheets rather than aggregation of nanowires or nanotubes. Instead of utilizing surfactants as soft templates to obtain mesoporous architectures, the high surface area of the crumpled boehmite nanosheets was achieved through the self-induced corrugations to prohibit the 2D material from serious stacking. Also, previous boehmite materials were prepared at environments above pH 4, mostly at weakly basic solutions; the low pH condition in our synthesis made it possible to limit the thickness to only a few nanometers.

3.9 Conversion into gamma-alumina

Boehmite materials are known to undergo isomorphous phase transformation to γ-alumina at high temperature.[12] Since our crumpled boehmite nanosheets were highly crumpled in three-dimension, one expects sintering can be avoided and nanosheets of γ-alumina can be obtained. Thus calcination of boehmites in air at 500-900 ℃ for 4 h was performed. All XRD patterns of the resulting materials can be indexed to face-centered cubic

γ-Al_2O_3 phase (Figure S10), and the diffraction peaks become more intense and sharper with increasing calcination temperature, showing improvement of crystallinity at higher temperature. The corresponding TEM images of the γ-alumina are shown in

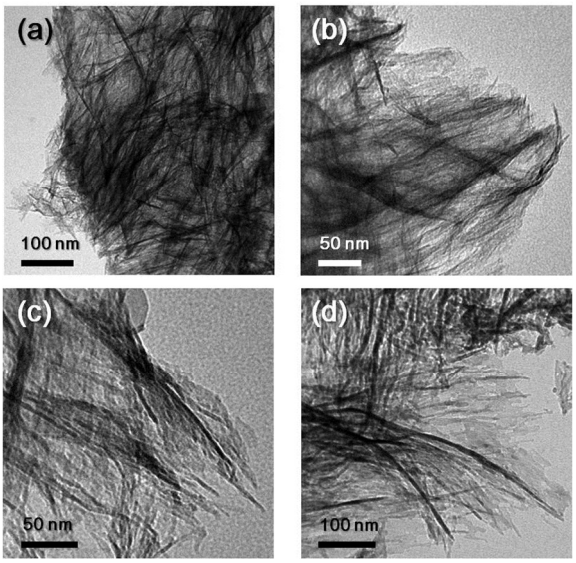

Fig. 9 TEM images of γ-alumina obtained by calcination of the crumpled boehmite nanosheets at (a) 500 ℃, (b) 600 ℃, (c) 700 ℃, and (d) 900 ℃.

Figure 9. Samples calcined at 500 ℃ and 600 ℃ (Figure 9a,b) show almost identical crumpled nanosheet morphology as the parent boehmite material. However, when the calcination temperature was raised to 700 ℃ (Figure 9c), the structure became partially discontinuous, resembling to aggregated nanowires. Moreover, a further increase of temperature to 900 ℃ made the discontinuity more evident (Figure 9d), the original crumpled nanosheets turned into nanowires connected by tattered nanosheets. During the conversion at 700 ℃ and 900 ℃, it was supposed that the dehydration of interlayer and surface H_2O led to severe shrinkage of volume,[48] which transformed the folds into the nanowires.

N_2 adsorption-desorption isotherms of the transformed alumina derived at 500 ℃ (Figure S11a) exhibits nearly the same isotherm and specific surface area as the original boehmite material. For sample calcined at 600 ℃ (Figure S11b), it displays type II isotherm but slightly different H3 type hysteresis loop. The desorption curve in the region around P/P_0 of 0.5 decreases smoothly instead of dropping abruptly, indicating the absence of pore blocking phenomenon. The calculated BET surface area is 298.6 m^2/g, over 90% of surface area is still remained. However, sample obtained at 900 ℃ reveals type II adsorption branch but with a narrow hysteresis at high relative pressure (Figure S11c). Furthermore, the surface area decreases to 143.7 m^2/g, less than half the surface area of crumpled boehmite nanosheets. It is commonly known that elevation of calcination temperature results in better crystallinity accompanied with decrease of surface area. The deformation of nanosheet structure at calcination temperature of 700 ℃ and 900 ℃ is thus expected, while the crumpled morphology are still preserved after moderate calcination at 500 ℃ and 600 ℃. A large amount of low-coordinated atoms or defects are anticipated to exist at the curved surface of folds and wrinkles over the crumpled alumina nanosheets. These surface atoms and defects are generally considered as active sites for catalytic reactions. Moreover, it has been reported that appropriate coverage of water molecules at the surface of γ-alumina is essential to initiate highly reactive defects,[49] the crumpled γ-alumina nanosheets obtained from boehmite nanosheets, at 500 ℃ and 600 ℃, may have great potential application in catalysis.

4. Conclusions

In this work, we have synthesized a boehmite of crumpled nanosheets with curtain-like morphology via a two-stage hydrothermal process. It has been demonstrated that the stage-1 hydrothermal treatment is to form aluminum hydroxide intermediate with a special core-shell structure which is the key to generate the curtain-like folds and wrinkles of the final product. In the stage-2 hydrothermal procedure, the hydroxide intermediate undergoes phase transformation to boehmite. The transformed boehmite shows nanosheet structure and becomes curtain-like crumpled due to the strain induced by the clustered cores, and the resulting morphology depends on the temperature condition in the second stage. It was the very low pH environment that made it possible to achieve the 2D materials with such thin thickness. The double lattice unit thickness and the crumpled structure contribute to the high specific surface area. The crumpled boehmite nanosheets can be further transformed to γ-alumina materials, while the curtain-like morphology and high surface area are preserved after calcination at moderate temperatures. Since boehmite has been illustrated to exhibit catalytic activity due to its weak Lewis acid sites,[50] both the boehmite and alumina of crumpled nanosheets will be of potential use in catalysis, adsorption, and separation applications.

Acknowledgements

This research was funded by National Taiwan University and the National Science Council of Taiwan.

Notes and references

[a] *Department of Chemistry, National Taiwan University, No.1 Sec 4, Roosevelt Road, Taipei 10617, Taiwan. Fax: +886 2-23660954; E-mail: cymou@ntu.edu.tw*
[b] *Center for Condensed Matter Sciences, National Taiwan University, No.1 Sec 4, Roosevelt Road, Taipei, 10617, Taiwan.*

† Electronic Supplementary Information (ESI) available: details of calculations of theoretical beohmite surface area; SEM images, FTIR spectra, and zeta-potentials of AlOOH samples in the growth evolution experiment; GC-MS results of the suspension and the controlled sample; dissolution of aluminum from boehmite in the leak test; N_2 sorption isotherms of boehmites prepared by different stage-1 treatments; XRD patterns and N_2 sorption isotherms of boehmites derived at different stage-2 hydrothermal temperatures; XRD patterns and N_2 sorption isotherms of aluminas calcined at different temperatures. See DOI: 10.1039/b000000x/.

1. N. Miyamoto and T. Nakato, *Isr. J. Chem.*, 2012, **52**, 881.
2. M. Osada and T. Sasaki, *Adv. Mater.*, 2012, **24**, 210.
3. D. Tunega, H. Pasalic, M. H. Gerzabek and H. Lischka, *J. Phys.: Condens. Matter*, 2011, **23**, 404201.
4. W. Q. Cai, J. G. Yu, B. Cheng, B. L. Su and M. Jaroniec, *J. Phys. Chem. C*, 2009, **113**, 14739.

5. L. Zhang, X. Jiao, D. Chen and M. Jiao, *Eur. J. Inorg. Chem.*, 2011, 5258.
6. X. Yang, X. Wang, Y. Feng, G. Zhang, T. Wang, W. Song, C. Shu, L. Jiang and C. Wang, *J. Mater. Chem. A*, 2013, **1**, 473.
7. X. X. Yu, J. G. Yu, B. Cheng and M. Jaroniec, *J. Phys. Chem. C*, 2009, **113**, 17527.
8. M. Logar, A. Kocjan and A. Dakskobler, *Mater. Res. Bull.*, 2012, **47**, 12.
9. Y. Yang, X. Zhao, Y. Zhu and F. Zhang, *Chem. Mater.*, 2012, **24**, 81.
10. A. Nakajima, A. Fujishima, K. Hashimoto and T. Watanabe, *Adv. Mater.*, 1999, **11**, 1365.
11. L. J. Liu, J. S. Zhao, Y. Zhang, F. Zhao and Y. B. Zhang, *J. Colloid Interface Sci.*, 2011, **358**, 277.
12. J. Zhang, S. Wei, J. Lin, J. Luo, S. Liu, H. Song, E. Elawad, X. Ding, J. Gao, S. Qi and C. Tang, *J. Phys. Chem. B*, 2006, **110**, 21680.
13. M. Digne, P. Sautet, P. Raybaud, P. Euzen and H. Toulhoat, *J. Catal.*, 2004, **226**, 54.
14. S. C. Shen, Q. Chen, P. S. Chow, G. H. Tan, X. T. Zeng, Z. Wang and R. B. H. Tan, *J. Phys. Chem. C*, 2007, **111**, 700.
15. T. He, L. Xiang and S. Zhu, *Langmuir*, 2008, **24**, 8284.
16. A. Dandapat and G. De, *J. Mater. Chem.*, 2010, **20**, 3890.
17. X. Y. Chen, H. S. Huh and S. W. Lee, *Nanotechnology*, 2007, **18**, 285608.
18. Y. Zhao, W. N. Martens, T. E. Bostrom, H. Y. Zhu and R. L. Frost, *Langmuir*, 2007, **23**, 2110..
19. D. B. Kuang, Y. P. Fang, H. Q. Liu, C. Frommen and D. Fenske, *J. Mater. Chem.*, 2003, **13**, 660.
20. H. W. Hou, Y. Xie, Q. Yang, Q. X. Guo and C. R. Tan, *Nanotechnology*, 2005, **16**, 741.
21. Y. Zhao, R. L. Frost, W. N. Martens and H. Y. Zhu, *Langmuir*, 2007, **23**, 9850.
22. Y. Liu, D. Ma, X. Han, X. Bao, W. Frandsen, D. Wang and D. Su, *Mater. Lett.*, 2008, **62**, 1297.
23. T. He, L. Xiang and S. Zhu, *CrystEngComm*, 2009, **11**, 1338.
24. P. d. S. Santos, A. C. Vieira Coelho, H. d. S. Santos and P. K. Kiyohara, *Mat. Res.*, 2009, **12**, 437.
25. S. Cho, J.-W. Jang, J. Park, S. Jung, S. Jeong, J. Kwag, J. S. Lee and S. Kim, *J. Mater. Chem. C*, 2013, **1**, 4497.
26. Y. Feng, W. Lu, L. Zhang, X. Bao, B. Yue, Y. Iv and X. Shang, *Cryst. Growth Des.*, 2008, **8**, 1426.
27. J. Zhang, S. Liu, J. Lin, H. Song, J. Luo, E. M. Elssfah, E. Ammar, Y. Huang, X. Ding, J. Gao, S. Qi and C. Tang, *J. Phys. Chem. B*, 2006, **110**, 14249.
28. M. Mazloumi, M. Attarchi, A. Lak, M. S. Mohajerani, A. Kajbafvala, S. Zanganeh and S. K. Sadrnezhaad, *Mater. Lett.*, 2008, **62**, 4184.
29. H. Liang, L. Liu, H. Yang, J. Wei, Z. Yang and Y. Yang, *CrystEngComm*, 2011, **13**, 2445.
30. G. Ji, M. Li, G. Li, G. Gao, H. Zou, S. Gan and X. Xu, *Powder Technol.*, 2012, **215-216**, 54.
31. J. Xiao, H. Ji, Z. Shen, W. Yang, C. Guo, S. Wang, X. Zhang, R. Fu and F. Ling, *Rsc Adv.*, 2014, **4**, 35077.
32. D. H. M. Buchold and C. Feldmann, *Nano Lett.*, 2007, **7**, 3489.
33. L. Zhang, W. Lu, L. Yan, Y. Feng, X. Bao, J. Ni, X. Shang and Y. Lv, *Microporous Mesoporous Mater.*, 2009, **119**, 208.
34. W. Q. Cai, J. G. Yu, S. H. Gu and M. Jaroniec, *Cryst. Growth Des.*, 2010, **10**, 3977.
35. L. Zhang, W. Lu, R. Cui and S. Shen, *Mater. Res. Bull.*, 2010, **45**, 429.
36. W. Q. Cai, H. Q. Li and Y. Zhang, *Mater. Chem. Phys.*, 2006, **96**, 136.
37. Z. Xu, J. Yu, J. Low and M. Jaroniec, *ACS Appl. Mater. Interfaces*, 2014, **6**, 2111.
38. S. P. Altaner, J. J. Fitzpatrick, M. D. Krohn, P. M. Bethke, D. O. Hayba, J. A. Goss and Z. A. Brown, *Am. Mineral.*, 1988, **73**, 145.
39. J. T. Kloprogge, H. Ruan and R. L. Frost, *J. Mater. Sci.*, 2001, **36**, 603.
40. F. Mercuri, D. Costa and P. Marcus, *J. Phys. Chem. C*, 2009, **113**, 5228.
41. Y. Xia, X. Jiao, Y. Liu, D. Chen, L. Zhang and Z. Qin, *J. Phys. Chem. C*, 2013, **117**, 15279.
42. D. Chiche, M. Digne, R. Revel, C. Chaneac and J.-P. Jolivet, *J. Phys. Chem. C*, 2008, **112**, 8524.
43. P. L. Chen and I. W. Chen, *J. Am. Ceram. Soc.*, 1993, **76**, 1577.
44. R. L. Frost, D. L. Wain, R. A. Wills, A. Musemeci and W. Martens, *Thermochim. Acta*, 2006, **443**, 56.
45. Y. Xia, B. Chen, X. Jiao and D. Chen, *Phys. Chem. Chem. Phys.*, 2014, **16**, 5866.
46. S. Castet, J. L. Dandurand, J. Schott and R. Gout, *Geochim. Cosmochim. Acta*, 1993, **57**, 4869.
47. Y. Watanabe, T. Kasama, K. Fukushi, T. Ikoma, Y. Komatsu, J. Tanaka, Y. Moriyoshi and H. Yamada, *Separ. Sci. Technol.*, 2011, **46**, 818.
48. T. Tsukada, H. Segawa, A. Yasumori and K. Okada, *J. Mater. Chem.*, 1999, **9**, 549.
49. R. Wischert, P. Laurent, C. Coperet, F. Delbecq and P. Sautet, *J. Am. Chem. Soc.*, 2012, **134**, 14430.
50. A. Takagaki, J. C. Jung and S. Hayashi, *Rsc Adv.*, 2014, **4**, 43785.

Table of Content

Boehmite and γ-Aumina nanosheets with curtain-like crumpled morphology have been synthesized via template-free hydrothermal process